Assembly of Fluorescent Polymer Nanoparticles using different Microfluidic Mixers

Huaiyou Chen,[a] *Ali Emre Celik,*[a‡] *Angela Mutschler,*[b‡] *Antoine Combes,*[a] *Anne Runser,*[a] *Andrey Klymchenko,*[a] *Sébastien Lecommandoux,**[b] *Christophe Serra,**[c] *Andreas Reisch**[a]

a: *Université de Strasbourg, CNRS, Laboratoire de Bioimagerie et Pathologies UMR 7021, Strasbourg F-67000, France; E-mail: reisch@unistra.fr.*

b: *Université Bordeaux, CNRS, Bordeaux INP, LCPO, UMR 5629, F-33600, Pessac, France; E-mail: lecommandoux@enscbp.fr.*

c: *Université de Strasbourg, CNRS, Institut Charles Sadron UPR 22, F-67000 Strasbourg, F-67000, France; E-mail: ca.serra@unistra.fr.*

† These authors contributed equally.

Abstract

Nanoprecipitation is a facile and efficient approach to the assembly of loaded polymer nanoparticles (NPs) for applications in bioimaging and targeted drug-delivery. Their successful use in clinics requires reproducible and scalable synthesis, for which microfluidics appears as an attractive technique. However, in the case of nanoprecipitation, particle formation depends strongly on mixing. Here, we compare 5 different types of microfluidic mixers with respect to the formation and properties of Poly(D-L-lactide-co-glycolide) (PLGA) and Poly(methyl methacrylate) NPs loaded with a fluorescent dye salt: a cross-shaped mixer, a multilamination mixer, a split & recombine mixer, two herringbone mixers, and two impact-jet mixers. Size and fluorescence properties of the NPs obtained with these mixers are evaluated. All mixers, except the cross-shaped one, yield NPs at least as small and fluorescent as those obtained manually. Notably in the case of impact-jet mixers operated at

high flow speeds, the size of the NPs could be strongly reduced from >50 nm down to <20 nm. Surprisingly, the fluorescence quantum yield of NPs obtained with these mixers also depends strongly on the flow speed, increasing, in the case of PLGA, from 30 to >70%. These results show the importance of precisely controlling the assembly conditions for loaded polymer NPs. The present work further provides guidance for choosing the optimal microfluidic set-up for production of nanomaterials for biomedical applications.

KEYWORDS: Microfluidics, Nanoparticle synthesis, Nanoprecipitation, Size control, Fluorescent nanoparticles

Introduction

Polymer nanoparticles (NPs) have attracted high interest in the biomedical field, notably as carriers for contrast agents and as systems for drug targeting and release.[1–3] They offer the possibility to use biocompatible or even biodegradable materials, present a high versatility in terms of material and load properties. Their surface properties can now be readily controlled, and through this their fate in biological environments. Over the last two decades, the development of polymer NPs has achieved a level, at which scale-up and reproducibility of particle assembly starts to become a focus, in order to translate this type of materials towards the clinic and commercialization.[4–7] As an example, so-called fluorescent dye-loaded polymer NPs have gained increasing interest as very bright fluorescent probes.[8–11] Thanks to different approaches for overcoming aggregation-caused quenching of the dyes inside the particles, they gave rise to fluorescent emitters several orders of magnitude brighter than fluorescent proteins, molecular dyes, or even luminescent quantum dots. These particle systems have already led to various applications, i.e. as ultrabright probes for single-particle tracking in vitro and in vivo,[12,13] cell labelling agents,[14] as well as light-harvesting nanomaterials for signal amplification,[15] and very sensitive probes for biomolecules.[16,17]

Polymer NPs can be synthesized either from monomers in various types of emulsion polymerizations or from already formed polymers.[18,19] Among the latter, nanoprecipitation is

a very attractive approach for the assembly of loaded polymer NPs.[20–22] In nanoprecipitation, both polymer and load are dissolved in a water miscible solvent and the resulting organic solution is added to an aqueous phase, which can or cannot contain surfactant molecules (Scheme 1). Mixing, and typically interdiffusion, of the organic and aqueous phase, leads to a mixture in which the polymer and the load are not soluble anymore, creating supersaturation, which is the driving force for particle formation. The fact that particle formation in this case is a kinetically controlled process allows trapping the load. This means that encapsulation (and release) of compounds inside polymer NPs is not only controlled by their chemistry and hence their equilibrium partitioning between particle and dispersant phase.[21,23] Indeed, encapsulation efficiency can also be optimized by adjusting the conditions of particle formation, independently of the nature of the loaded cargo.

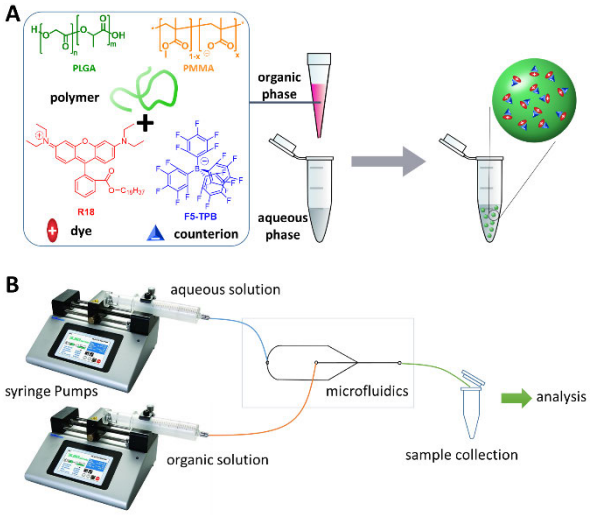

Scheme 1. (A) "Manual" preparation of NPs, showing the structures of the polymers (PLGA: n = m; PMMA: x=0.[illegible] , the dye with its counterion, and the principle of nanoprecipitation. (B) Microfluidics set-up used for the preparation of NPs (except for Split and recombine).

Originally, nanoprecipitation was mainly performed through manual addition of one of the phases to the other, typically with the aqueous phase in large excess.[24] Taking into account the fact that often relatively small amounts of valuable compounds have to be encapsulated, one possibility to better control the addition of the two phases is the use of microfluidics.[9,25–29] Microfluidics should, in principle, allow automatization of NP assembly with high

reproducibility and further scale-up through highly parallel synthesis. However, particle formation in nanoprecipitation depends strongly on the speed of mixing of the two phases, which defines the supersaturation and the homogeneity of conditions during particle formation. In classical microfluidic systems the flow is strongly laminar due to the small dimensions of the channels (corresponding to low Reynolds number). In consequence, mixing is mainly relying on diffusion, which is a slow process resulting in a very low speed of mixing. To circumvent this problem, different types of microfluidic mixers have been developed, making use of external energy input (active mixers) or relying solely on pressure driven flow (passive mixers).[30,31] Among the latter, three major strategies exist to increase the speed of mixing: (i) Decrease of the width of the laminar flow phases, resulting in a decrease in the diffusion distances. This principle is notably realized in hydrodynamic flow focusing,[32] multilaminar mixers,[33,34] but also in so-called split & (re)combine mixers.[35] (ii) Introduction of transversal flow elements, leading to partially chaotic mixing, as in the case of staggered herringbone mixers.[36,37] (iii) Collision of the flows, leading to a further breakdown into small fluid segments and, in some cases, to actual turbulent mixing, as in impact-jet and vortex mixers.[38–42]

Application of such mixers to the assembly of polymer NPs through nanoprecipitation has, effectively, proven to be a useful approach to reduce the size and, in several cases, the polydispersity of the resulting particles, with a great reproducibility.[43] However, up to now direct comparisons of the performance of these different mixers are scarce,[26,39,44,45] and, in particular, to the best of our knowledge, no such comparison addresses the assembly of fluorescent dye-loaded polymer NPs through nanoprecipitation. In the present work, we therefore evaluated the fabrication of dye-loaded polymer NPs using different microfluidic mixers (Figure 1) for two polymers frequently used for the preparation of NPs: Poly(D-L-lactide-co-glycolide) (PLGA) and Poly(methyl methacrylate) (PMMA) (Scheme 1). Both

polymers contained small amounts of carboxylic acid groups, on the chain end for PLGA and as co-monomer (1.3 mol%) for PMMA, to better control particle size.[46] These polymers were loaded with the salt of a rhodamine B derivative (R18) with the bulky hydrophobic counterion tetrakis(pentafluorophenyl)borate (F5-TPB). Besides its practical significance for reducing aggregation caused quenching (ACQ), this dye salt has the advantage that it can serve as a model compound, whose fluorescence directly reflects the organization of the load inside the NP.[47] We first compared the sizes of NPs obtained from these polymers either through manual nanoprecipitation or using one of seven different microfluidic mixers while varying the flow conditions over a wide range of flow speeds. For selected systems, we then evaluated in more detail the fluorescence properties.

Experimental

Materials

Poly(D-L-lactide-co-glycolide) (PLGA, acid terminated, lactide:glycolide=50:50, Mw 24,000-38,000 $g.mol^{-1}$, Ref.: 719870, Lot: BCBV0402) and Poly(methyl methacrylate-co-methacrylic acid) (PMMA, Mw 34,000 $g.mol^{-1}$, Mn 15,000 $g.mol^{-1}$, 1.3 % methacrylic acid, Ref.: 376914, Lot: 02314EJV) were purchased from Sigma Aldrich. Acetonitrile (analytical reagent ≥99.5%) was obtained from Carlo-Erba; R18/F5-TPB was synthesized from rhodamine B octadecyl ester perchlorate (Sigma Aldrich, >98.0%) and lithium tetrakis(pentafluorophenyl)borate ethyl etherate (AlfaAesar, 97%) through ion exchange followed by purification through column chromatography as described previously.[47] MilliQ water was used in all experiments.

Methods

Preparation of NPs: Stock solutions of polymers were prepared at a concentration of 10 $g.L^{-1}$ in acetonitrile. These solutions were diluted to 2 $g.L^{-1}$ in acetonitrile containing 5 wt% of R18/F5-TPB (relative to the polymer), where needed. In some cases these solutions were further diluted to 1 or 0.5 $g.L^{-1}$. For manual preparation, this solution was quickly added to a

9-fold volume excess of MilliQ water under shak ng (Thermomixer comfort, Eppendorf, 0 rpm at 2 C). For preparation using microfluidics, this solution was mixed in the microfluidic mixer in a ratio 1:9 with MilliQ water at various flow rates. The latter were chosen over the range, where a reproducible and stable flow was achieved with the corresponding mixer. Samples were taken after about 30 s of stabilization at the given flow rates. The particle solutions were analyzed directly after suitable dilution, without purification in order to better visualize the effects of preparation conditions.

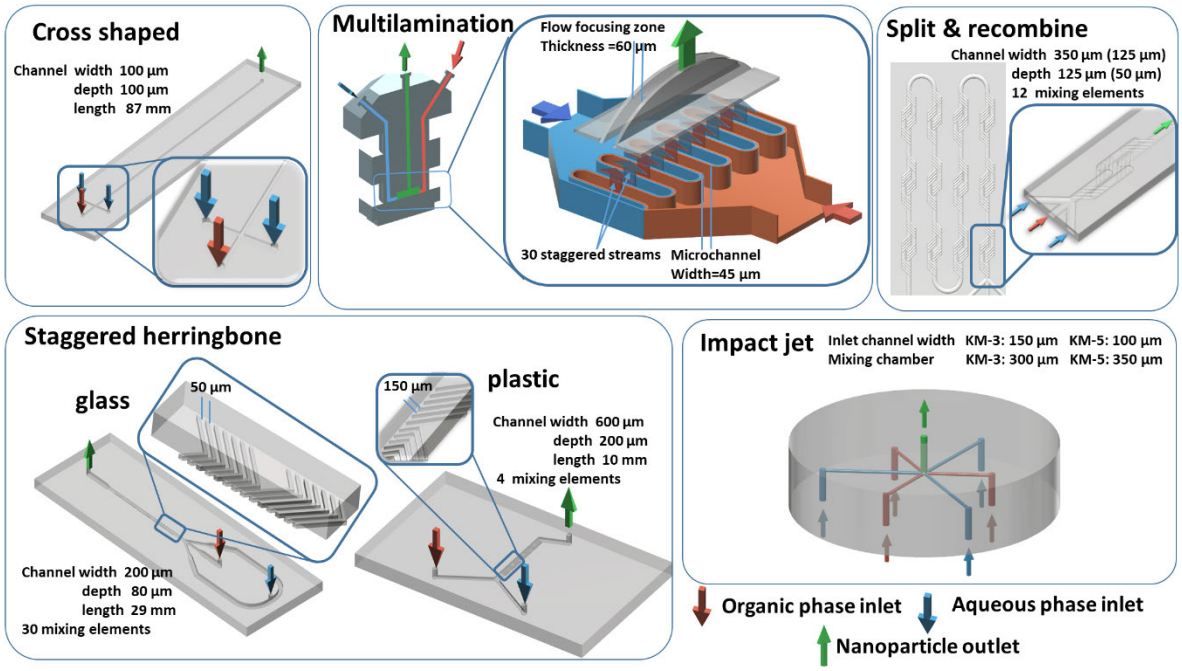

Figure 1. Overview of mixers used here for nanoparticle preparation.

Microfluidics set-up: Two setups were used: For the split and recombine mixer, we used a Dolomite™ Microfluidics system based on two pressure pumps, two flowmeters and a micromixer chip of 2 mixing stages. One pump was connected to the chip through the first and third inputs using a T-connector. The other pump was directly link d to the chip through the second input. Pump calibration were made for acetonitrile and water. For all other mixers we used two KDS Legato™ 0 Infuse Only Syringe Pumps from KD Scientific to control

the flow in the organic and aqueous flow line independently. Mixing of the two phases is carried out in the corresponding mixers (see below), and the samples were then collected from the outlet of the mixers in Eppendorf tubes (Scheme 1).

The following mixers were used for particle preparation (Figure 1, SI Scheme S1): A Zeonor (plastic) cross-shaped mixer with a channel width of 100 µm from Microfluidic ChipShop (Ref.: 10000237). A Zeonor staggered herringbone mixer with a rectangular cross-section of width 600 µm and height 200 µm from Microfluidic ChipShop (Ref.: 10000076). A glass staggered herringbone mixer from Darwin Microfluidics (Ref.: 012.00-4264). A high pressure interdigital multilamination mixer with 15 channels per fluid entry of 45 µm width (HPIMM, IMM, Mainz, Germany).[48] Two impact-jet mixers (KM-3 and KM-5 respectively, Fujifilm Corporation, Kyoto, Japan) whose structure consists of three steel plates, namely the inlet, mixing and outlet plates. Both inlet fluid streams are split into 3 or 5 sub-streams thanks to microchannels of 150 or 100 µm, respectively. Then the alternated 6 or 10 sub-streams converge to a single pine hole of 300 or 350 µm, respectively, where they are mixed by frontal collision.

Dynamic light scattering (DLS): The sizes of NPs were measured on a Zetasizer Nano series ZS for NPs prepared using the split & recombine mixer and on a Zetasizer Nano series ZSP (Malvern Instruments S.A.) for all other preparations. DLS measurements were performed directly after NP preparation without further dilution at concentrations of 0.05 - 0.2 $g.L^{-1}$. For size determination, each sample was measured 10 times with a run length of 10 s each. The measurement position was fixed to 4.3 mm and the attenuation was adjusted automatically. The volume average values were used, which are determined by the Zetasizer software (Malvern) based on Mie theory. Mean values give the average over at least three independent preparations, error bars correspond to the standard deviation over the means from different preparations.

Transmission electron microscopy (TEM): Solutions of bare dye-loaded NPs (5µL) were deposited onto carbon-coated copper−rhodium electron microscopy grids following amylamine glow-discharge. They were then treated for 20 s with a 2% uranyl acetate solution for staining. The obtained grids were observed using a Tecnai F20 Twin transmission electron microscope (FEI Eindhoven Holland) operating at a voltage of 200 kV. Images (2,048 pixels × 2,048 pixels) were recorded using a US1000 camera (Gatan). After drying, the uranyl acetate remaining on the sample provides the contrast, often negative, but in some cases also in the form of a ring or shadow around the particles. Images were analyzed using the Fiji software. At least 200 particles per condition were analyzed.

Absorption and emission spectra were recorded on a Cary 5000 Scan ultraviolet–visible spectrophotometer (Varian) and on a FS5 Spectrofluorometer (Edinburgh Instruments) equipped with a thermostated cell compartment, respectively. For nanoparticles formed with the split and recombine mixer, absorption and emission spectra were recorded on a UV double beam spectrophotometer (Specord 200 plus, analytikjena) equipped with a D_2E and a Halogen Lamp and a Jasco FP-Spectrofluorometer with a Xe arc lamp with a shielded lamp housing (150 W). The excitation wavelength was set to 530 nm and emission was recorded from 540 to 750 nm. QYs were determined from the absorbance values at the excitation wavelength ($A_{x,530nm}$) and the integral over the whole emission range (F_x) using a simplified relative method. , with rhodamine 101 in ethanol as reference (QY = 0.95, absorbances below 0.1))., according to the formula

$$QY_{NP} = QY_{r101}\frac{F_{NP}A_{NP,530nm}n_{H_2O}^2}{F_{r101}A_{r101,530nm}n_{EtOH}^2}$$

Where NP corresponds to solutions of the nanoparticles in water and r101 to rhodamine 101 in ethanol and n corresponds to the respective refractive indices of the solvents (1.33 for water and 1.36 for ethanol).

Results and Discussion

Size

In a first step, PLGA and PMMA NPs were prepared "manually" by adding quickly solutions of the polymers in acetonitrile at 2 $g.L^{-1}$ to a 9-fold excess of MilliQ water under shaking. This resulted in particles with sizes of 51 (±5) nm and 77 (±5) nm, respectively, for PLGA and PMMA, as determined by dynamic light scattering (DLS). DLS results showed relatively low polydispersity indices (PDI) of 0.14 (±0.03) and 0.07 (±0.02), in good agreement with results obtained previously.[46] We then used the same solutions for the preparation of NPs using microfluidic mixers, where the organic to aqueous phase ratio was adjusted through the volume flow rates in a ratio 1:9. In the following, we first present the obtained sizes and their flow rate dependencies for the individual mixers, and will then compare and discuss the specific influences of the different mixers. It should be noted that the obtained NPs by manual and microfluidics assisted nanoprecipitation were stable over the time frame of the experiments, that is for at least one week.

The simplest mixer we used was a cross-shaped mixer, in which the two lateral inlets were fed with the aqueous phase, while the organic phase entered through the central inlet, with a long, mixing channel of 100 µm x 100 µm cross-section. This configuration leads to hydrodynamic flow focusing with the initial width of the organic phase being determined through the channel width and the ratios of flow rates. Here, this should correspond to a width of about 10 µm (as confirmed using confocal microscopy). The sizes of PLGA NPs obtained in this configuration were all larger than 100 nm, showed strong batch to batch variations, and had a tendency to become bigger with increasing flow rate (Figure 2 A). In the case of PMMA, frequent blocking of the mixer was observed, and no consistent results could be obtained. Observation of the mixer under the microscope showed indeed deposits inside the channel.

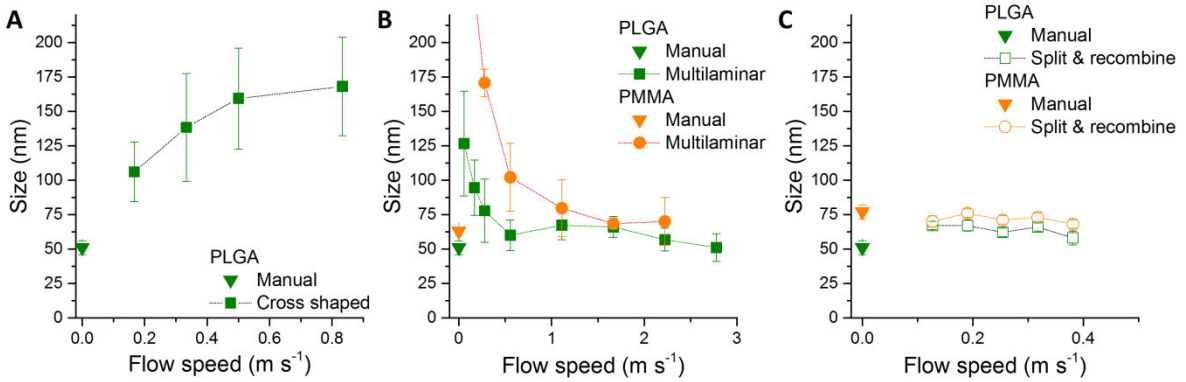

Figure 2. Size of NPs obtained using (A) the cross-shaped, (B) the multilamination, and (C) the split & (re)combine mixers as a function of flow speed as measured by DLS. Polymer concentrations in the organic phase were 2 g.L^{-1}, except for PMMA in the case of the multilamination mixer (and the corresponding manual preparation), where the concentration was reduced to 0.5 g.L^{-1} to avoid clogging. The values correspond to the mean of the volume average from at least three measurements. Error bars give the standard deviation.

A further decrease of the initial width of the organic layer can be achieved by employing the multilamination mixer. Here, we used a multilamination mixer having 15 interdigitated microchannels with a width of 45 µm each (HPIMM). The size of PLGA NPs obtained using this mixer decreased with increasing flow speed from around 90 nm at low speed until a plateau value is reached around 60 nm, which is slightly below the size of NPs obtained manually (Figure 2B). In the case of PMMA, again frequent issues of blocking occurred. However, in the case of the multilamination mixer, it was possible to overcome these by reducing the concentration of the PMMA in the organic phase to 0.5 g.L^{-1}. At low flow speed, very large NPs with sizes above 600 nm were obtained, but the size of the particles decreased quickly with increasing flow-speed to reach about 70 nm. Manual preparation of NPs using PMMA at 0.5 g.L^{-1} yielded NPs of 68 nm, smaller than particles prepared from 2 g.L^{-1} (77 nm), and also slightly smaller than the particles prepared using the multilamination mixer.

An approach to further improve the mixing is to split the flow in several sub-flows, to recombine the flows, and then to split and recombine them again several times. Using such a split & (re)combine mixer resulted for both, PLGA and PMMA, in NP sizes that were nearly

independent of flow speed (over the studied range, Figure 2 C). The resulting particle sizes were around θ nm and Ø nm for PLGA and PMMA, respectively, and thus relatively close. PLGA particles were slightly bigger and PMMA particles slightly smaller than corresponding particles prepared manually.

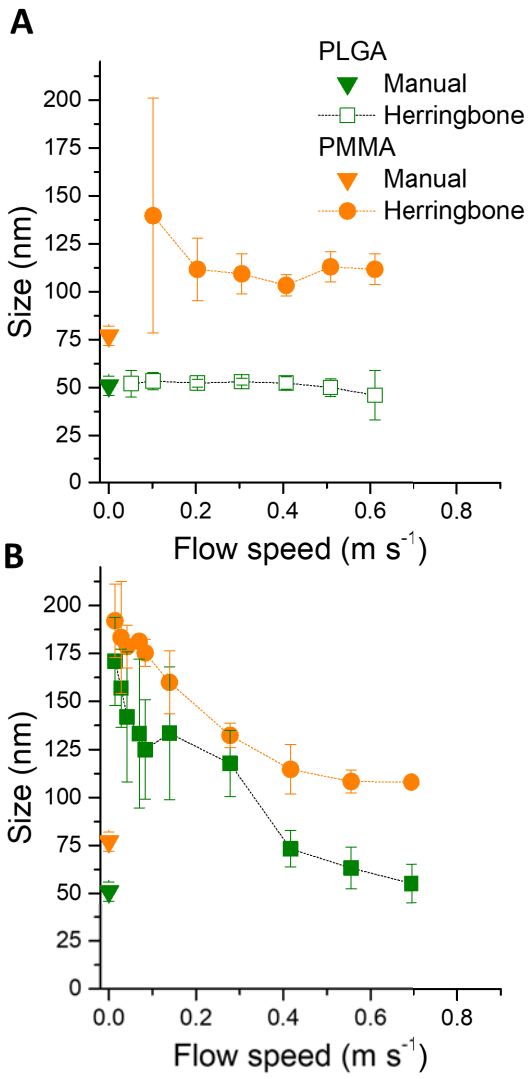

Figure 3. Size of NPs obtained using (A) the glass and (B) the plastic staggered herringbone mixer as a function of flow speed as measured by DLS. The values correspond to the mean of the volume average from at least three measurements. Error bars give the standard deviation.

A different way to improve mixing between the two phases in microfluidics is to induce a lateral flow component, which leads to vortices or “chaotic elements” within the flow that further decrease the thickness of the phases. Such lateral flows can be achieved, for example,

using ridges or grooves in the channel walls, giving rise to the so-called staggered herringbone mixer.[36] Here, we used two versions of herringbone mixers: a plastic based system bearing 4 mixing-blocks and a channel cross-section of 600 µm x 200 µm, and a glass based systems bearing 30 mixing-blocks and a channel cross-section of 200 µm x 80 µm. Interestingly, the dependence of the particle size on flow speed was very different in both cases (Figure 3): while in the case of the glass herringbone mixer the size was practically independent of flow speed over the studied range, there was a clear decrease in size with increasing flow speed for the plastic herringbone mixer. In the latter case, the particle sizes at low flow speeds were close to 200 nm for both polymers. At the highest flow speeds, the sizes decreased to around 50 nm and 110 nm for PLGA and PMMA, respectively, and thus to values close to those obtained with the glass herringbone mixer. Compared to manual preparation, the achievable sizes using herringbone mixers were hence slightly lower for PLGA and significantly bigger for PMMA.

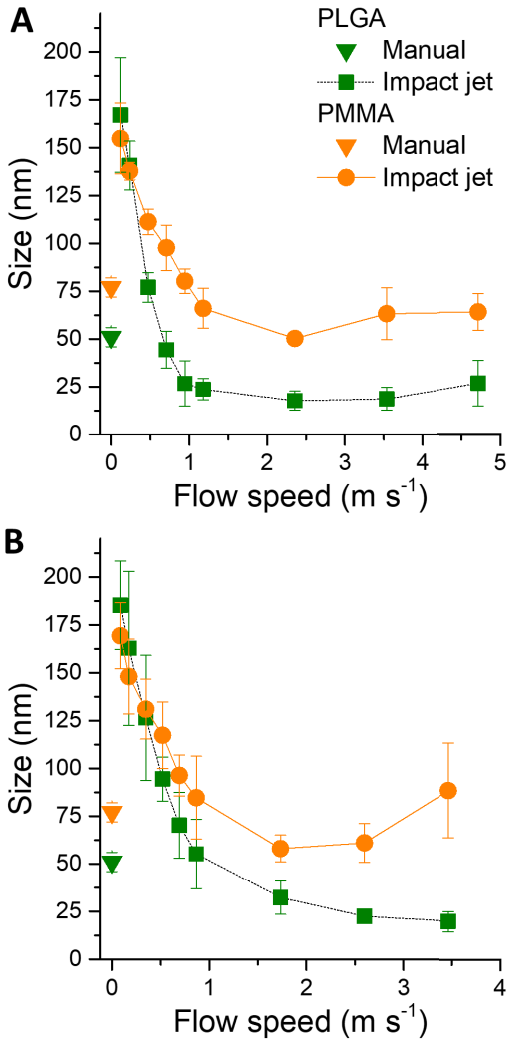

Figure 4 Size of NPs obtained using (A) the KM-3 and (B) KM-5 impact jet mixers as a function of flow speed as measured by DLS. The values correspond to the mean of the volume average from at least three measurements. Error bars give the standard deviation.

Another possibility to overcome laminar flow in microfluidics is to use so-called impact jet, impinging jet or vortex mixers, in which collision of the flows leads to turbulent behavior. Here, we tested two impact jet mixers (KM-3 and KM-5). For both mixers, and for both polymers, the particle size depended strongly on the flow speed (Figure 4). In all cases, particle sizes obtained at low flow speeds were of the order of 100 nm, close to those observed for the plastic herringbone mixer, the cross-shaped mixer and, at least partially, for the multilamination mixer at low flow speed. With increasing flow speed, we observed a steep decrease in particle size, which was more expressed for PLGA than for PMMA, and for the

former somewhat faster with the KM-3 mixer. In the case of PMMA, a minimum particle size of around 50 nm (slightly bigger for the KM-5 mixer) was achieved at intermediate flow speed, followed by a slight increase in particle size. The latter was accompanied by increased batch to batch variations, which might be a sign of instabilities of the system. For PLGA, the particle sizes decreased down to a plateau at 20 nm for the KM-3 mixer, a value that was also obtained for the PLGA NPs produced with the KM-5 mixer at the highest flow speeds. The sizes of PLGA and PMMA NPs prepared either at low (0.24 m s^{-1}) or high (2.3 m s^{-1}) flow speed were further measured as a function of time and compared to NPs prepared manually (SI, Table S3) . No significant changes in size were observed, indicating that the preparation method had no influence on stability.

For one of the impact-jet mixers (KM-3) , we further determined the z-potential obtained at low and high flow rates (SI, Table S2) . In all cases, the z-potentials were clearly negative, with higher absolute values (around -30 mV) for PLGA than for PMMA (around -20 mV). Interestingly, no significant influence of the flow rate was observed, and the values were close to those of NPs obtained through manual preparation.

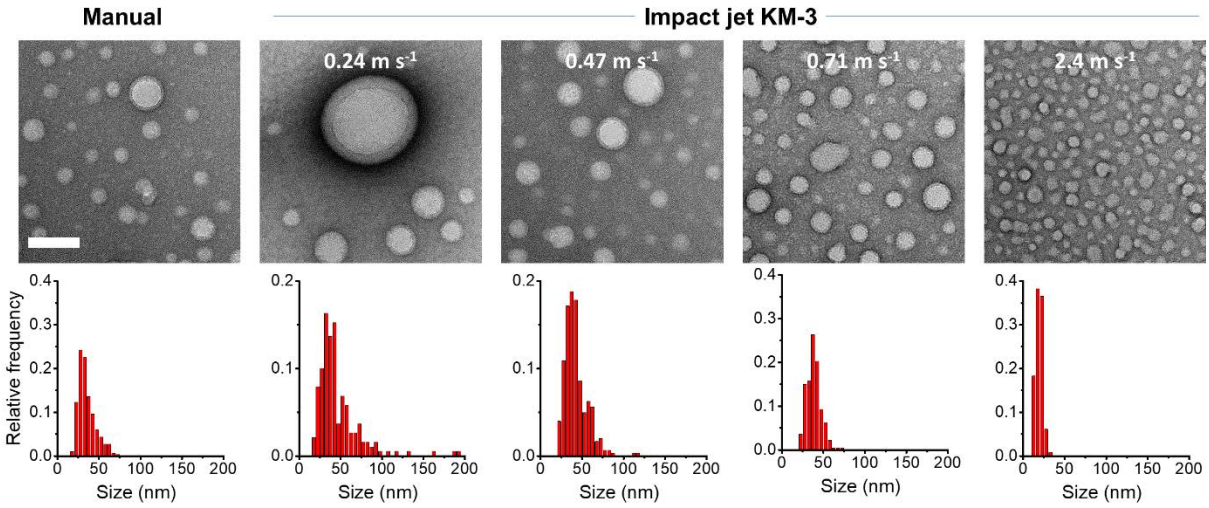

Figure 5. Analysis of PLGA NPs using TEM. Representative TEM images for different conditions of particle preparation are given above (scale bar corresponds to 100 nm), and the particle size distributions as obtained from >200 articles per condition are given below.

Selected NPs were then further analyzed using transmission electron microscopy (TEM), with respect to their size and their size distribution (Figure 5, Table 1, SI Figure S1). In all cases, the sizes obtained by TEM were smaller than those obtained by DLS, as observed previously.[12] This difference can be attributed first of all to the fact that DLS measures the hydrodynamic diameter, while TEM gives the hard sphere diameter. A second reason for this difference is that the intensity of scattering increases strongly with the size of the scattering particles.[49] In consequence, larger particles contribute stronger to the results obtained in DLS. Considering PLGA NPs, we observed, in general, a good agreement between the trends observed by TEM and DLS, notably the strong decrease in particle size for the impact jet mixers with flow speed. A closer look at the particle size distribution obtained from TEM indicates that two processes contribute to this decrease: (i) At low flow speed a significant amount of very large particles was obtained with sizes larger than 100 and even reaching 200 nm. The fraction and sizes of these large particles decreased in the flow speed range of 0.06 – 0.12 $m.s^{-1}$, and at higher values they were practically entirely absent. (ii) At the same time, the size corresponding to the maximum (mode) of the distribution was relatively stable over this range of flow speeds, but decreased strongly when going to high flow speeds (here 0.6 $m.s^{-1}$). For the latter, a particularly narrow particle size distribution was observed and practically no particles larger than 30 nm were detected. In the case of PLGA NPs prepared using the multilamination mixer, the size distribution was similar to what was observed for manual preparation of NPs. For those prepared by the herringbone (glass) mixer the mean value of particle size (and the mode) were slightly higher.

In the case of PMMA NPs, both the mean sizes and the width of the size distributions, as obtained by TEM, were clearly larger than for PLGA NPs prepared in corresponding conditions. For example, in samples prepared manually or at low flow speed in the impact jet mixer, a large number of particles > 50 nm and > 100 nm, respectively, were detected. At

high speed, the PMMA particles prepared with the impact jet mixer appeared often not clearly separated, but rather as chains in TEM. Taken into account the diameter of single “beads”, a mean size of only 20 nm was obtained, compared to 50 nm measured by DLS. A possible explanation could be that smaller PMMA NPs are more prone to aggregation due to the higher hydrophobicity of PMMA. This is also in good agreement with the observed instabilities at the highest flow rates for PMMA (see above).

Table 1. Comparison of particle sizes obtained from DLS and TEM.

Polymer	Mixer	Flow speed [m s^{-1}]	Mean size	
			DLS [nm]	TEM[a] [nm]
PLGA	Manual	-	51 ± 5	37 ± 8
	Herringbone (glass)	0.31	46 ± 13	47 ± 12
	Multilamination	2.2	57 ± 9	39 ± 10
	Impact jet KM-3	0.24	141 ± 13	47 ± 15
		0.47	77 ± 8	43 ± 11
		0.71	44 ± 10	38 ± 8
		2.4	18 ± 5	20 ± 5
PMMA	Manual		77 ± 5	63 ± 15
	Impact jet KM-3	0.24	138 ± 5	98 ± 25
		2.4	50 ± 3	22 ± 7

[a)] Given are the mean values over > 200 particles ± the width of the distribution at half maximum.

A comparison of the smallest particles that could be assembled with each mixer for each polymer is given in Figure 6. A first observation is that in all cases PLGA particles were smaller than PMMA particles made under the same conditions. A second observation is that “manual” particle preparation performs quite well with respect to most of the microfluidic mixers that were tested. Indeed, in the case of PLGA, the smallest particle sizes that could be obtained using split & (re)combine, multilamination, and herringbone mixers are with 45 nm to 57 nm close to those obtained manually (51 ± 5 nm). However, two remarkable exceptions exist: the cross-shaped mixer gave much larger particles (> 100 nm), and the impact jet

mixers gave clearly smaller particles with sizes going below 20 nm. In the case of PMMA, differences were more clearly marked: no reproducible particle preparation was achieved using the cross-shaped mixer. The herringbone mixers gave bigger particles than manual preparation, while the multilamination and the split & combine mixers gave slightly smaller NPs, approaching the size of the particles made from PLGA. A specific case for PMMA is the impact jet mixer. It gave again the smallest particles, however, there was a large discrepancy between the results obtained from DLS (60 nm) and TEM (20 nm).

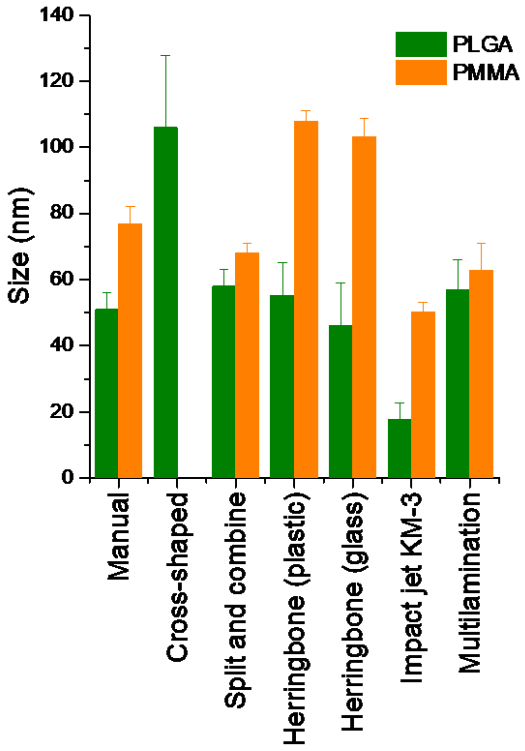

Figure 6. The sizes of the smallest PLGA and PMMA NPs obtained using the different mixers are given as measured by DLS. The values correspond to the mean of the volume average over at least three independent preparations. Error bars give the standard deviation

In the case of relatively rapid mixing, nanoprecipitation is generally considered to occur via a nucleation and growth mechanism, in which supersaturation acts as a driving force that enables formation of nuclei, which then grow through incorporation of "monomers" (single polymer, dye, or drug molecules), but also through aggregation of particles.[20,50–52] The final particle size and size distribution then depends on the relative rates of nucleation, growth, and

aggregation, with small particles being formed at high nucleation, low growth and very low aggregation rates. Stabilization from aggregation can typically be achieved through the implementation of charged groups on the particle surface, e.g. using polymers with a low percentage of charged groups as was the case here.[46,53,54] Both, nucleation and growth depend on supersaturation, but the nucleation rate increases more rapidly with increasing supersaturation.[20,52] As the supersaturation depends on the state of mixing during particle formation, the mixing time (notably compared to the time scale of particle formation) is generally considered to be of high importance for the particle formation in nanoprecipitation.[20,26]

Let us leave aside the nature of the polymer for the moment and concentrate on one polymer (e.g. PLGA). In this case, supersaturation depends on the speed and quality of mixing of the two phases: the faster the mixing, the higher the water fraction and in consequence the supersaturation at the beginning of particle formation (in first approximation). The cross-shaped mixer, which gave the biggest particles can, indeed, be considered to have the lowest mixing speed, relying largely on diffusion over a relatively long distance. At the same time, the contact of the organic phase with the walls can also lead to adsorption of polymer and further perturb particle formation (in agreement with the strong batch to batch variation), an issue that can be addressed by using 3 dimensional hydrodynamic flow focusing.[27,55] Particle sizes obtained with the multilamination and split & (re)combine mixers were markedly smaller, with relatively little dependence on flow speed, which can be attributed to a strong decrease of the diffusion length and so an increase in mixing speed. However, especially at higher flow velocities, a contribution of turbulences to mixing is also possible.[33] The two herringbone mixers showed different dependencies of particle size on flow speed: while in the case of the plastic based mixer with 4 mixing elements particle sizes depended strongly on the flow speed, the glass based mixer with 30 mixing elements did not

show such a dependence. This indicates that in the case of a lower number of mixing elements additional flow events (like turbulences at the entry or outlet) are important for efficient mixing that depend on the flow speed, while this is not the case if sufficient mixing elements are used. However, differences in the adsorption of the polymers on the wall materials could also have an influence.

All these mixers gave particle sizes close to those obtained "manually", indicating that the achieved mixing times lie in a similar range. In the case of the impact jet mixers, the collision of the flows leads to very high shear rates that help break-up of the flow in small fluid segments.[40] (Reynolds numbers remain, however, below 2000 at the used flow parameters indicating that the flow does not become turbulent.) Previous studies have shown that for this type of mixer the mixing performance indeed increased with increasing fluid velocities,[40,42] which should correspond to decreasing mixing times of the aqueous and organic phase with increasing flow speed, and to particular short mixing times for this kind of mixer. This can then explain the decrease in particle size observed here: as noted above, faster mixing times should lead to particle formation at higher water to solvent ratios (and so also higher supersaturation) and lower solid concentrations. Both conditions have been shown previously to lead to the formation of smaller particles.[12,50] At the same time, increasing nucleation speed should also narrow the size distribution, as it leads to distinct nucleation and growth phases, with all the particles growing at the same time.[20,52] Here, TEM images indicated a particular narrow size distribution for particles assembled at high flow speeds in impact jet mixers. Taken together, the previous studies and the results obtained here indicate that in the impact jet mixers, the fastest mixing can be reached among the microfluidic mixers tested here, probably close to those achieved in other types of impact jet or vortex mixers.[38,39,56]

The bigger particle sizes observed for PMMA compared to PLGA can be attributed to its higher hydrophobicity. Indeed, in a systematic study we found that particle size in the case of

manual nanoprecipitation correlated with hydrophobicity of the used polymers.[57] Possible reasons for this are a decrease in nucleation rate with increasing surface tension of the formed particles,[20,52] and a stronger tendency of particle aggregation. The higher hydrophobicity of PMMA is also thought to be related to its more pronounced tendency for clogging the microfluidic mixers through adsorption on the mixer surfaces, notably in the case of the cross-shaped but also for the multilamination mixer. The case of the herringbone mixers requires a further comment: Indeed, the difference in size between PLGA and PMMA appeared to be particularly strong. However, it should be noted that for the cross-shaped and the multilamination mixer, synthesis of PMMA NPs was not feasible at standard conditions due to clogging (in the case of the multilamination mixer, PMMA NP assembly was possible at reduced concentration). This underlines the high difficulty to synthesize PMMA NPs using microfluidic mixers, probably due to a combination of increased aggregate formation and stronger adsorption of the polymer on the wall. The only two mixers performing quite well for PMMA were the split-and-recombine and the impact jet mixers. A particular case was observed for PMMA particles made using the impact jet mixers at high flow speeds: both DLS and TEM results showed that in this way the smallest PMMA NPs were achieved. However, the obtained values, 50 nm by DLS and 22 nm by TEM were clearly different. At the same time, the TEM images revealed “chains” of very small PMMA NPs. A possible explanation for this discrepancy is that the impact jet mixer at high flow speeds yields very small NPs, both for PLGA and PMMA. In the case of PMMA, these very small NPs could show a stronger tendency to aggregate than in the case of PLGA, leading to an increase in the sizes observed by DLS. However, it cannot be excluded that the “aggregation” only occurs on the grids for TEM imaging. Here, MilliQ water was used for nanoprecipitation, however, it is known that ionic force and pH can also influence particle formation.[12,15,46,53] It would

therefore be interesting to subsequently study the combined effects of precipitation medium and mixing in the future.

Fluorescence

In a next step, we then evaluated the microfluidic mixers for the assembly of fluorescent dye-loaded NPs. For this, 5 wt% (relative to the polymer) of the dye salt R18/F5-TPB were added to the polymer solution and nanoprecipitation was performed as before by mixing with a nine-fold excess of MilliQ water (Scheme 1). The association of the hydrophobic rhodamine derivative R18 with the bulky hydrophobic counterion F5-TPB has been shown previously to lead to very efficient encapsulation (>90% loading efficiency) in various polymer NPs.[46,58] At the same time the counterion acts as spacer insulating the fluorophores and reducing aggregation caused quenching (ACQ), which allows achieving NPs of very high brightness.

Nanoprecipitation of solutions containing the polymer and the dye salt yielded pink, transparent solutions with no visible signs of aggregate formation. Absorbance spectra of the dye loaded NPs prepared manually and using different microfluidic mixers were, generally, very similar in intensity and close to the expected values (SI Figure S4, the details of the shape of the spectra are discussed below). Together with previous results obtained on similar systems this indicates efficient encapsulation of the dye salt in the polymer particles.[47,58] Here, we then further concentrated on the influence of the different mixers on the brightness of the obtained NPs, which is given by the product of the absorbance and the quantum yield (QY). QY is the ratio of the photons emitted as fluorescence to the absorbed photons, and as the dye concentration is kept constant here, and so were the absorbances, the QY is the decisive factor determining brightness.

Manual preparation of dye-loaded NPs yielded PLGA NPs with a QY of 42 ± 6 % and PMMA NPs with a QY of 80 ± 5 %, in good agreement with previous results.[47] At the same time the sizes of these NPs increased to, respectively, 91 and 99 nm for PLGA and PMMA

upon addition of R8 F5-TPB (compared to 5 and 7 nm, respectively, without dye salt). This increase could be related to the association of some of the R8 with negative charges on the particle surface, as observed previously.[58] We then evaluated the QYs of PLGA particles obtained under the conditions giving the smallest NPs for the multilamination and herringbone mixers (Figure S3). QYs for all three were about 0 %, i.e. close to those obtained manually. The obtained particle sizes were also similar, except for the plastic herringbone mixer, which gave larger particles (Figure S2). In the case of the split & (re)combine mixer both, size and QY, were of the order of those of the corresponding NPs obtained manually. However, a slight increase in QY and decrease in size with flow speed was observed for both, PLGA and PMMA (Figure S3). A still stronger influence of the mixing process was observed for impact jet mixers (here we concentrated on KM-3 mixer, Figure 7 : for PLGA particles, we observed a continuous increase in the QY with increasing flow speed, going from less than 5% at the lowest flow speed to over 70% at the highest speed tested, where the increase seemed to level off (Figure 7 . For PMMA particles, on the other hand, we observed a slight decrease of the QY from 92 to 72 % over the same flow speed range. At the same time, the particle sizes decreased with flow speed, as observed for the pure polymer particles, reaching 23 nm and 53 nm for PLGA and PMMA NPs, respectively at the highest flow rates (Figure S2).

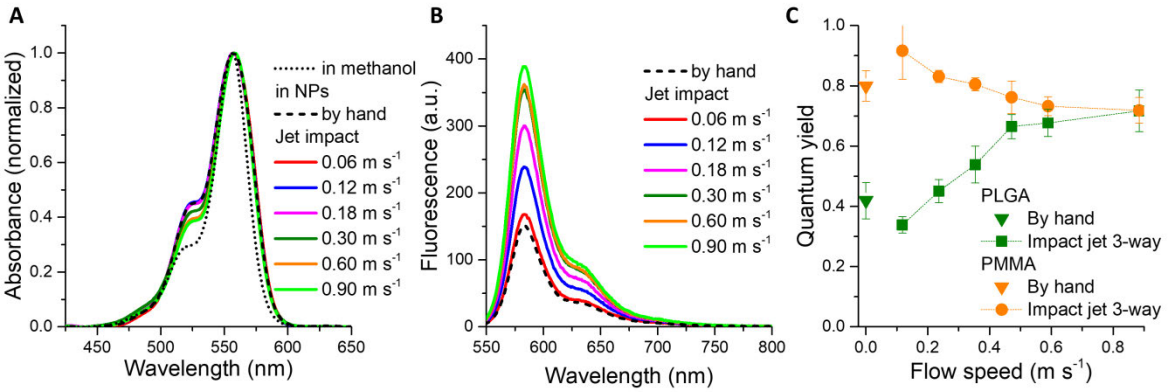

Figure 7 Absorption (A) and emission spectra (B) of PLGA NPs with 5 wt% of R8 F5-TPB prepared manually or using the impact jet mixer KM-3 at different flow speeds. Absorption

spectra in (A) are normalized to visualize changes in their shape; the spectra of the dye salt in methanol is given for comparison. The emission spectra in (B) are all recorded using the same settings and for the same global fluorophore concentration. (C) Quantum yields (QY) for PLGA and PMMA NPs with 5 wt% of R18/F5-TPB prepared manually or using the impact jet mixer at different flow speeds. Average values over at least three independent preparations are given and the error bars correspond to the standard deviation.

In order to understand the striking increase in QY for PLGA NPs, a close observation of the corresponding absorption and emission spectra provides a better picture of the changes occurring with flow rate: in the case of PLGA, the absorption spectra showed only slight variations in the maximum absorbance (<10%, Figure S4). This also indicates that the preparation method did not influence significantly the efficiency of dye encapsulation. Indeed, the absorbance was very close to that observed for manual NP preparation, for which an encapsulation efficiency >90% was previously found.[58] However, a relative decrease of the intensity of the shoulder at 530 nm with respect to the maximum was clearly observed with increasing flow speed (Figure 7A). Such a spectral change indicates a decrease in aggregation of the dyes inside the NPs.[47,59] At the same time the intensity of fluorescence increased steadily with increasing flow speed (Figure 7B), corresponding to the observed strong increase in QY. In the case of PMMA (Figure S4, S5), no major changes of the intensity and shape of the absorption spectra were detected (except for the lowest flow speed, where absorbance was about 20% lower). Here, the absolute intensity of the maximum and the relative intensity of the shoulder at 530 nm of the dye loaded in NPs were close to what is observed for the same dye in solution, indicating optimal encapsulation and minimal aggregation, and only a slight decrease in the emission with flow speed was measured.

The smaller QY of R18 in PLGA compared to PMMA was attributed previously to a clustering of the dyes within PLGA in contrast to a more homogeneous distribution in PMMA due to the lower hydrophobicity of PLGA.[47] Here, we found that QY in PLGA NPs increased with increasing flow speed, suggesting that a better or faster mixing of the two phases leads to

less clustering or aggregation of the dyes. The observed decreasing relative intensity of the shoulder in the absorbance spectra, attributed to dye dimers or aggregates, points indeed in this sense. A possible reason for such differences in organization could be that at faster mixing of the two phases, particle formation occurs at higher supersaturations, at which PLGA and dye salt precipitate faster, leaving no time for clustering of the dye salt. The opposite behavior in the case of the PMMA particles could be due to the fact that for faster mixing the dye salt is exposed to a medium with higher water fraction before being incorporated into particles, which could favor dissociation of the ion pair. Overall, faster mixing decreases the difference between the two polymers in terms of dye encapsulation and aggregation, so that the spectroscopic properties of the obtained NPs become similar.

Conclusions

Our evaluation of the use of microfluidics for the preparation of polymer NPs, and in particular fluorescent dye-loaded NPs, has shown that microfluidics is indeed a very powerful approach for reproducible synthesis of nanomaterials. Microfluidics offer notably the possibility to produce NPs in continuous flow, facilitating high quality synthesis of large amounts, and it could be further scaled-up through parallel fabrication. Comparing different microfluidic mixers, relying on very different mixing principles, showed that most of these performed at least as well as “manual” preparation in terms of achievable particle size and fluorescence properties. In particular, impact jet mixers allowed strongly decreasing the size of NPs made from both PLGA and PMMA, achieving even particles below 20 nm for the former.

This was attributed to a strongly enhanced mixing speed. At the same time the impact-jet mixer also allowed strongly increasing the fluorescence QY for PLGA NPs and, in consequence, the brightness of these particles, simply by tuning the mixing speed. Apart from the interest of achieving brighter fluorescence markers, this finding is of high importance for

other fields using loaded polymer NPs. Indeed, the increase in fluorescence was attributed to changes in the encapsulation of the load. Tailoring the distribution of the load by simple variation of the flow conditions is expected to present important possibilities in the design of drug delivery systems.

Author Contributions

The manuscript was written through contributions of all authors. All authors have given approval to the final version of the manuscript. ‡These authors contributed equally.

Conflicts of interest

There are no conflicts of interest to declare.

Supporting Information

Detailed results of dynamic light scattering, further electron microscopy images, additional spectra and figures on size and quantum yields of dye-loaded polymer nanoparticles.

Acknowledgements

This work was supported by the ANR JC/JC grant “Supertrack” ANR-16-CE09-0007, by an FRC Emerging Investigators grant, by the ERC Consolidator grant BrightSens 648528, and by the “Prix Espoirs de l’Université de Strasbourg”. The authors acknowledge the support and the use of resources of the French Infrastructure for Integrated Structural Biology FRISBI ANR-10-INBS-05 and of Instruct-ERIC and especially C. Crucifix for help with electron microscopy.

References

(1) Wang, Y.; Feng, L.; Wang, S. Conjugated Polymer Nanoparticles for Imaging, Cell Activity Regulation, and Therapy. *Adv. Funct. Mater.* **2019**, *29* (5), 1806818. https://doi.org/https://doi.org/10.1002/adfm.201806818.

(2) Shi, J.; Kantoff, P. W.; Wooster, R.; Farokhzad, O. C. Cancer Nanomedicine: Progress, Challenges and Opportunities. *Nat. Rev. Cancer* **2017**, *17* (1), 20–37. https://doi.org/10.1038/nrc.2016.108.

(3) Pearce, A. K.; O’Reilly, R. K. Insights into Active Targeting of Nanoparticles in Drug Delivery: Advances in Clinical Studies and Design Considerations for Cancer Nanomedicine. *Bioconjug. Chem.* **2019**, *30* (9), 2300–2311. https://doi.org/10.1021/acs.bioconjchem.9b00456.

(4) Wang, L.; Wang, J. Self-Assembly of Colloids Based on Microfluidics. *Nanoscale* **2019**, *11* (36), 16708–16722. https://doi.org/10.1039/c9nr06817a.

(5) Roces, C. B.; Christensen, D.; Perrie, Y. Translating the Fabrication of Protein-Loaded Poly(Lactic-Co-Glycolic Acid) Nanoparticles from Bench to Scale-Independent Production Using Microfluidics. *Drug Deliv. Transl. Res.* **2020**, *10* (3), 582–593. https://doi.org/10.1007/s13346-019-00699-y.

(6) Ma, Q.; Cao, J.; Gao, Y.; Han, S.; Liang, Y.; Zhang, T.; Wang, X.; Sun, Y. Microfluidic-Mediated Nano-Drug Delivery Systems: From Fundamentals to Fabrication for Advanced Therapeutic Applications. *Nanoscale* **2020**, *12* (29), 15512–15527. https://doi.org/10.1039/D0NR02397C.

(7) Hamdallah, S. I.; Zoqlam, R.; Erfle, P.; Blyth, M.; Alkilany, A. M.; Dietzel, A.; Qi, S. Microfluidics for Pharmaceutical Nanoparticle Fabrication: The Truth and the Myth. *Int. J. Pharm.* **2020**, *584*, 119408. https://doi.org/10.1016/j.ijpharm.2020.119408.

(8) Reisch, A.; Klymchenko, A. S. Fluorescent Polymer Nanoparticles Based on Dyes: Seeking Brighter Tools for Bioimaging. *Small* **2016**, *12* (15), 1968–1992. https://doi.org/10.1002/smll.201503396.
(9) Visaveliya, N. R.; Köhler, J. M. Softness Meets with Brightness: Dye-Doped Multifunctional Fluorescent Polymer Particles via Microfluidics for Labeling. *Adv. Opt. Mater.* **2021**, *9* (13), 2002219. https://doi.org/10.1002/adom.202002219.
(10) Wan, Q.; Huang, Q.; Liu, M.; Xu, D.; Huang, H.; Zhang, X.; Wei, Y. Aggregation-Induced Emission Active Luminescent Polymeric Nanoparticles: Non-Covalent Fabrication Methodologies and Biomedical Applications. *Appl. Mater. Today* **2017**, *9*, 145–160. https://doi.org/10.1016/j.apmt.2017.06.004.
(11) Robin, M. P.; O'Reilly, R. K. Strategies for Preparing Fluorescently Labelled Polymer Nanoparticles. *Polym. Int.* **2015**, *64* (2), 174–182. https://doi.org/10.1002/pi.4842.
(12) Egloff, S.; Runser, A.; Klymchenko, A.; Reisch, A. Size-Dependent Electroporation of Dye-Loaded Polymer Nanoparticles for Efficient and Safe Intracellular Delivery. *Small Methods* **2021**, *5* (2), 2000947. https://doi.org/10.1002/smtd.202000947.
(13) Khalin, I.; Heimburger, D.; Melnychuk, N.; Collot, M.; Groschup, B.; Hellal, F.; Reisch, A.; Plesnila, N.; Klymchenko, A. S. Ultrabright Fluorescent Polymeric Nanoparticles with a Stealth Pluronic Shell for Live Tracking in the Mouse Brain. *Acs Nano* **2020**, *14* (8), 9755–9770. https://doi.org/10.1021/acsnano.0c01505.
(14) Andreiuk, B.; Reisch, A.; Lindecker, M.; Follain, G.; Peyriéras, N.; Goetz, J. G.; Klymchenko, A. S. Fluorescent Polymer Nanoparticles for Cell Barcoding In Vitro and In Vivo. *Small* **2017**, *13* (38), 1701582. https://doi.org/10.1002/smll.201701582.
(15) Trofymchuk, K.; Reisch, A.; Didier, P.; Fras, F.; Gilliot, P.; Mely, Y.; Klymchenko, A. S. Giant Light-Harvesting Nanoantenna for Single-Molecule Detection in Ambient Light. *Nat. Photonics* **2017**, *11* (10), 657. https://doi.org/10.1038/s41566-017-0001-7.
(16) Egloff, S.; Melnychuk, N.; Reisch, A.; Martin, S.; Klymchenko, A. S. Enzyme-Free Amplified Detection of Cellular MicroRNA by Light-Harvesting Fluorescent Nanoparticle Probes. *Biosens. Bioelectron.* **2021**, *179*, 113084. https://doi.org/10.1016/j.bios.2021.113084.
(17) Lone, M. S.; Bhat, P. A.; Afzal, S.; Chat, O. A.; Dar, A. A. Energy Transduction through FRET in Self-Assembled Soft Nanostructures Based on Surfactants/Polymers: Current Scenario and Prospects. *Soft Matter* **2021**, *17* (3), 425–446. https://doi.org/10.1039/D0SM01625J.
(18) Rao, J. P.; Geckeler, K. E. Polymer Nanoparticles: Preparation Techniques and Size-Control Parameters. *Prog. Polym. Sci.* **2011**, *36* (7), 887–913. https://doi.org/10.1016/j.progpolymsci.2011.01.001.
(19) Banik, B. L.; Fattahi, P.; Brown, J. L. Polymeric Nanoparticles: The Future of Nanomedicine. *Wiley Interdiscip. Rev. Nanomed. Nanobiotechnol.* **2016**, *8* (2), 271–299. https://doi.org/10.1002/wnan.1364.
(20) D'Addio, S. M.; Prud'homme, R. K. Controlling Drug Nanoparticle Formation by Rapid Precipitation. *Adv. Drug Deliv. Rev.* **2011**, *63* (6), 417–426. https://doi.org/10.1016/j.addr.2011.04.005.
(21) Martínez Rivas, C. J.; Tarhini, M.; Badri, W.; Miladi, K.; Greige-Gerges, H.; Nazari, Q. A.; Galindo Rodríguez, S. A.; Román, R. Á.; Fessi, H.; Elaissari, A. Nanoprecipitation Process: From Encapsulation to Drug Delivery. *Int. J. Pharm.* **2017**, *532* (1), 66–81. https://doi.org/10.1016/j.ijpharm.2017.08.064.
(22) Sanson, C.; Schatz, C.; Le Meins, J.-F.; Soum, A.; Thévenot, J.; Garanger, E.; Lecommandoux, S. A Simple Method to Achieve High Doxorubicin Loading in

Biodegradable Polymersomes. *J. Control. Release Off. J. Control. Release Soc.* **2010**, *147* (3), 428–435. https://doi.org/10.1016/j.jconrel.2010.07.123.

(23) Hayward, R. C.; Pochan, D. J. Tailored Assemblies of Block Copolymers in Solution: It Is All about the Process. *Macromolecules* **2010**, *43* (8), 3577–3584. https://doi.org/10.1021/ma9026806.

(24) Fessi, H.; Puisieux, F.; Devissaguet, J. P.; Ammoury, N.; Benita, S. Nanocapsule Formation by Interfacial Polymer Deposition Following Solvent Displacement. *Int. J. Pharm.* **1989**, *55* (1), R1–R4. https://doi.org/10.1016/0378-5173(89)90281-0.

(25) Ding, S.; Anton, N.; Vandamme, T. F.; Serra, C. A. Microfluidic Nanoprecipitation Systems for Preparing Pure Drug or Polymeric Drug Loaded Nanoparticles: An Overview. *Expert Opin. Drug Deliv.* **2016**, *13* (10), 1447–1460. https://doi.org/10.1080/17425247.2016.1193151.

(26) Liu, Y.; Yang, G.; Zou, D.; Hui, Y.; Nigam, K.; Middelberg, A. P. J.; Zhao, C.-X. Formulation of Nanoparticles Using Mixing-Induced Nanoprecipitation for Drug Delivery. *Ind. Eng. Chem. Res.* **2020**, *59* (9), 4134–4149. https://doi.org/10.1021/acs.iecr.9b04747.

(27) Khan, I. U.; Serra, C. A.; Anton, N.; Vandamme, T. F. Production of Nanoparticle Drug Delivery Systems with Microfluidics Tools. *Expert Opin. Drug Deliv.* **2015**, *12* (4), 547–562. https://doi.org/10.1517/17425247.2015.974547.

(28) Liu, D.; Zhang, H.; Fontana, F.; Hirvonen, J. T.; Santos, H. A. Current Developments and Applications of Microfluidic Technology toward Clinical Translation of Nanomedicines. *Adv. Drug Deliv. Rev.* **2018**, *128*, 54–83. https://doi.org/10.1016/j.addr.2017.08.003.

(29) Sun, Z.; Wu, B.; Ren, Y.; Wang, Z.; Zhao, C.-X.; Hai, M.; Weitz, D. A.; Chen, D. Diverse Particle Carriers Prepared by Co-Precipitation and Phase Separation: Formation and Applications. *ChemPlusChem* **2021**, *86* (1), 49–58. https://doi.org/https://doi.org/10.1002/cplu.202000497.

(30) Mansur, E. A.; Ye, M.; Wang, Y.; Dai, Y. A State-of-the-Art Review of Mixing in Microfluidic Mixers. *Chin. J. Chem. Eng.* **2008**, *16* (4), 503–516. https://doi.org/10.1016/S1004-9541(08)60114-7.

(31) Ward, K.; Fan, Z. H. Mixing in Microfluidic Devices and Enhancement Methods. *J. Micromechanics Microengineering Struct. Devices Syst.* **2015**, *25* (9). https://doi.org/10.1088/0960-1317/25/9/094001.

(32) Karnik, R.; Gu, F.; Basto, P.; Cannizzaro, C.; Dean, L.; Kyei-Manu, W.; Langer, R.; Farokhzad, O. C. Microfluidic Platform for Controlled Synthesis of Polymeric Nanoparticles. *Nano Lett.* **2008**, *8* (9), 2906–2912. https://doi.org/10.1021/nl801736q.

(33) Bally, F.; Garg, D. K.; Serra, C. A.; Hoarau, Y.; Anton, N.; Brochon, C.; Parida, D.; Vandamme, T.; Hadziioannou, G. Improved Size-Tunable Preparation of Polymeric Nanoparticles by Microfluidic Nanoprecipitation. *Polymer* **2012**, *53* (22), 5045–5051. https://doi.org/10.1016/j.polymer.2012.08.039.

(34) Yus, C.; Arruebo, M.; Irusta, S.; Sebastián, V. Microflow Nanoprecipitation of Positively Charged Gastroresistant Polymer Nanoparticles of Eudragit® RS100: A Study of Fluid Dynamics and Chemical Parameters. *Materials* **2020**, *13* (13), 2925. https://doi.org/10.3390/ma13132925.

(35) Bresseleers, J.; Bagheri, M.; Lebleu, C.; Lecommandoux, S.; Sandre, O.; Pijpers, I. A. B.; Mason, A. F.; Meeuwissen, S.; Nostrum, C. F. van; Hennink, W. E.; Hest, J. C. M. van. Tuning Size and Morphology of MPEG-b-p(HPMA-Bz) Copolymer Self-Assemblies Using Microfluidics. *Polymers* **2020**, *12* (11), 2572. https://doi.org/10.3390/polym12112572.

(36) Stroock, A. D.; Dertinger, S. K. W.; Ajdari, A.; Mezić, I.; Stone, H. A.; Whitesides, G. M. Chaotic Mixer for Microchannels. *Science* **2002**, *295* (5555), 647–651. https://doi.org/10.1126/science.1066238.

(37) Sanchez-Gaytan, B. L.; Fay, F.; Hak, S.; Alaarg, A.; Fayad, Z. A.; Pérez-Medina, C.; Mulder, W. J. M.; Zhao, Y. Real-Time Monitoring of Nanoparticle Formation by FRET Imaging. *Angew. Chem. Int. Ed.* **2017**, *56* (11), 2923–2926. https://doi.org/10.1002/anie.201611288.

(38) Markwalter, C. E.; Prud'homme, R. K. Design of a Small-Scale Multi-Inlet Vortex Mixer for Scalable Nanoparticle Production and Application to the Encapsulation of Biologics by Inverse Flash NanoPrecipitation. *J. Pharm. Sci.* **2018**, *107* (9), 2465–2471. https://doi.org/10.1016/j.xphs.2018.05.003.

(39) Johnson, B. K.; Prud'homme, R. K. Chemical Processing and Micromixing in Confined Impinging Jets. *AIChE J.* **2003**, *49* (9), 2264–2282. https://doi.org/10.1002/aic.690490905.

(40) Nagasawa, H.; Aoki, N.; Mae, K. Design of a New Micromixer for Instant Mixing Based on the Collision of Micro Segments. *Chem. Eng. Technol.* **2005**, *28* (3), 324–330. https://doi.org/https://doi.org/10.1002/ceat.200407118.

(41) Han, H.; Yoon, J. H.; Yi, G.-R.; Choi, W. I.; Lim, J.-M. High-Speed Continuous Production of Polymeric Nanoparticles with Improved Stability Using a Self-Aligned Coaxial Turbulent Jet Mixer. *J. Ind. Eng. Chem.* **2021**, *97*, 411–416. https://doi.org/10.1016/j.jiec.2021.02.025.

(42) Anton, N.; Bally, F.; Serra, C. A.; Ali, A.; Arntz, Y.; Mely, Y.; Zhao, M.; Marchioni, E.; Jakhmola, A.; Vandamme, T. F. A New Microfluidic Setup for Precise Control of the Polymer Nanoprecipitation Process and Lipophilic Drug Encapsulation. *Soft Matter* **2012**, *8* (41), 10628–10635. https://doi.org/10.1039/c2sm25357g.

(43) Lebleu, C.; Rodrigues, L.; Guigner, J.-M.; Brûlet, A.; Garanger, E.; Lecommandoux, S. Self-Assembly of PEG-b-PTMC Copolymers: Micelles and Polymersomes Size Control. *Langmuir* **2019**, *35* (41), 13364–13374. https://doi.org/10.1021/acs.langmuir.9b02264.

(44) Abdelkarim, M.; Abd Ellah, N. H.; Elsabahy, M.; Abdelgawad, M.; Abouelmagd, S. A. Microchannel Geometry vs Flow Parameters for Controlling Nanoprecipitation of Polymeric Nanoparticles. *Colloids Surf. Physicochem. Eng. Asp.* **2021**, *611*, 125774. https://doi.org/10.1016/j.colsurfa.2020.125774.

(45) Li, W.; Chen, Q.; Baby, T.; Jin, S.; Liu, Y.; Yang, G.; Zhao, C.-X. Insight into Drug Encapsulation in Polymeric Nanoparticles Using Microfluidic Nanoprecipitation. *Chem. Eng. Sci.* **2021**, *235*, 116468. https://doi.org/10.1016/j.ces.2021.116468.

(46) Reisch, A.; Runser, A.; Arntz, Y.; Mély, Y.; Klymchenko, A. S. Charge-Controlled Nanoprecipitation as a Modular Approach to Ultrasmall Polymer Nanocarriers: Making Bright and Stable Nanoparticles. *ACS Nano* **2015**, *9* (5), 5104–5116. https://doi.org/10.1021/acsnano.5b00214.

(47) Reisch, A.; Trofymchuk, K.; Runser, A.; Fleith, G.; Rawiso, M.; Klymchenko, A. S. Tailoring Fluorescence Brightness and Switching of Nanoparticles through Dye Organization in the Polymer Matrix. *ACS Appl. Mater. Interfaces* **2017**, *9* (49), 43030–43042. https://doi.org/10.1021/acsami.7b12292.

(48) Ding, S.; Serra, C. A.; Anton, N.; Yu, W.; Vandamme, T. F. Production of Dry-State Ketoprofen-Encapsulated PMMA NPs by Coupling Micromixer-Assisted Nanoprecipitation and Spray Drying. *Int. J. Pharm.* **2019**, *558*, 1–8. https://doi.org/10.1016/j.ijpharm.2018.12.031.

(49) Stetefeld, J.; McKenna, S. A.; Patel, T. R. Dynamic Light Scattering: A Practical Guide and Applications in Biomedical Sciences. *Biophys. Rev.* **2016**, *8* (4), 409–427. https://doi.org/10.1007/s12551-016-0218-6.

(50) Saad, W. S.; Prud'homme, R. K. Principles of Nanoparticle Formation by Flash Nanoprecipitation. *Nano Today* **2016**, *11* (2), 212–227. https://doi.org/10.1016/j.nantod.2016.04.006.

(51) Lepeltier, E.; Bourgaux, C.; Couvreur, P. Nanoprecipitation and the "Ouzo Effect": Application to Drug Delivery Devices. *Adv. Drug Deliv. Rev.* **2014**, *71*, 86–97. https://doi.org/10.1016/j.addr.2013.12.009.

(52) Mora-Huertas, C. E.; Fessi, H.; Elaissari, A. Influence of Process and Formulation Parameters on the Formation of Submicron Particles by Solvent Displacement and Emulsification–diffusion Methods: Critical Comparison. *Adv. Colloid Interface Sci.* **2011**, *163* (2), 90–122. https://doi.org/10.1016/j.cis.2011.02.005.

(53) Zhang, C.; Pansare, V. J.; Prud'homme, R. K.; Priestley, R. D. Flash Nanoprecipitation of Polystyrene Nanoparticles. *Soft Matter* **2011**, *8* (1), 86–93. https://doi.org/10.1039/C1SM06182H.

(54) Morozova, T. I.; Lee, V. E.; Panagiotopoulos, A. Z.; Prud'homme, R. K.; Priestley, R. D.; Nikoubashman, A. On the Stability of Polymeric Nanoparticles Fabricated through Rapid Solvent Mixing. *Langmuir* **2019**, *35* (3), 709–717. https://doi.org/10.1021/acs.langmuir.8b03399.

(55) Rhee, M.; Valencia, P. M.; Rodriguez, M. I.; Langer, R.; Farokhzad, O. C.; Karnik, R. Synthesis of Size-Tunable Polymeric Nanoparticles Enabled by 3D Hydrodynamic Flow Focusing in Single-Layer Microchannels. *Adv. Mater.* **2011**, *23* (12), H79–H83. https://doi.org/https://doi.org/10.1002/adma.201004333.

(56) Liu, Y.; Cheng, C.; Liu, Y.; Prud'homme, R. K.; Fox, R. O. Mixing in a Multi-Inlet Vortex Mixer (MIVM) for Flash Nano-Precipitation. *Chem. Eng. Sci.* **2008**, *63* (11), 2829–2842. https://doi.org/10.1016/j.ces.2007.10.020.

(57) Rosiuk, V.; Runser, A.; Klymchenko, A.; Reisch, A. Controlling Size and Fluorescence of Dye-Loaded Polymer Nanoparticles through Polymer Design. *Langmuir* **2019**, *35* (21), 7009–7017. https://doi.org/10.1021/acs.langmuir.9b00721.

(58) Andreiuk, B.; Reisch, A.; Bernhardt, E.; Klymchenko, A. S. Fighting Aggregation-Caused Quenching and Leakage of Dyes in Fluorescent Polymer Nanoparticles: Universal Role of Counterion. *Chem. – Asian J.* **2019**, *14* (6), 836–846. https://doi.org/10.1002/asia.201801592.

(59) Macdonald, R. I. Characteristics of Self-Quenching of the Fluorescence of Lipid-Conjugated Rhodamine in Membranes. *J. Biol. Chem.* **1990**, *265*, 13533–13539.

Supplementary Information

Assembly of Fluorescent Polymer Nanoparticles using different Microfluidic Mixers

Huaiyou Chen, Ali Emre Celik, Angela Mutschler, Antoine Combes, Anne Runser, *Andrey Klymchenko, Sébastien Lecommandoux,* Christophe Serra,* Andreas Reisch**

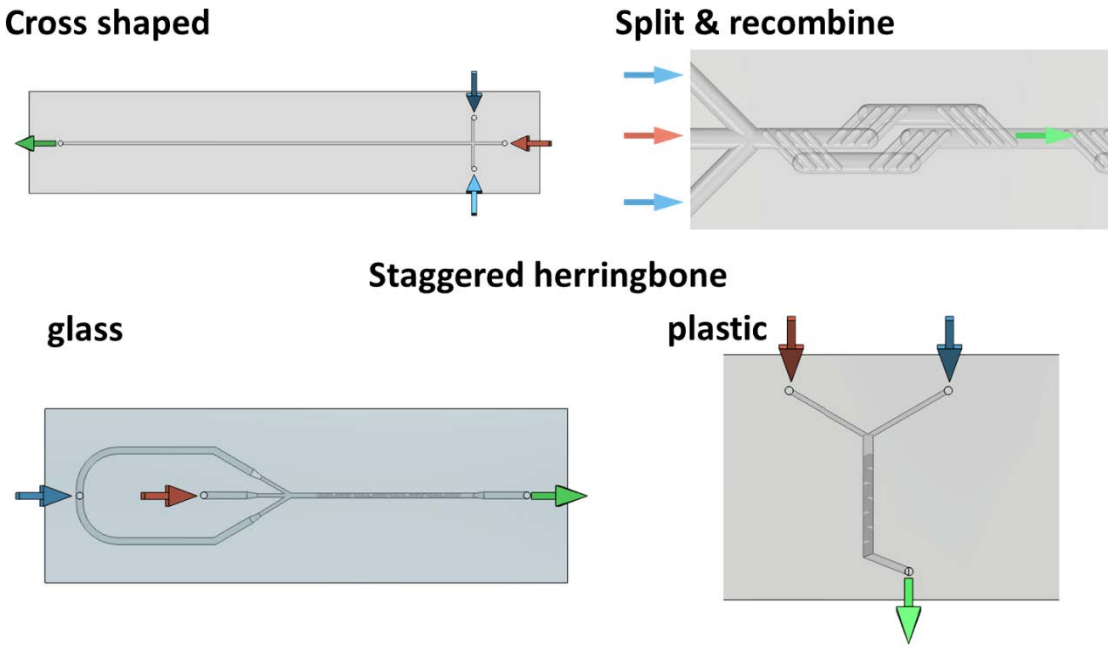

Scheme S1. Top-view of some of the mixers used here for nanoparticle preparation.

Table S1. Detailed DLS data for PLGA and PMMA NPs prepared using different micromixers.

Mixer	Flow speed	PLGA		PMMA	
	($m.s^{-1}$)	Size (nm)	PDI	Size (nm)	PDI
Manual	-	51 ± 5	0.14 ± 0.04	77 ± 5	0.07 ± 0.02
Cross-shaped	0.17	106 ± 22	0.18 ± 0.04	-	-
	0.33	138 ± 40	0.19 ± 0.03	-	-
	0.50	159 ± 37	0.17 ± 0.05	-	-
	0.83	168 ± 36	0.18 ± 0.06	-	-
Multilaminar	0.06	127 ± 38	0.09 ± 0.02	604 ± 325	0.29 ± 0.14
	0.17	95 ± 21	0.14 ± 0.02	236 ± 77	0.31 ± 0.12
	0.28	78 ± 23	0.22 ± 0.01	171 ± 11	0.24 ± 0.11
	0.56	60 ± 12	0.26 ± 0.03	102 ± 24	0.23 ± 0.06
	1.11	67 ± 11	0.29 ± 0.01	78 ± 21	0.22 ± 0.07
	1.67	66 ± 8	0.32 ± 0.02	68 ± 5	0.32 ± 0.05
	2.22	57 ± 9	0.26 ± 0.03	70 ± 17	0.31 ± 0.20
	2.78	51 ± 10	0.11 ± 0.03	-	-
Split & combine	0.13	67 ± 3	0.10 ± 0.04	70 ± 4	0.15 ± 0.12
	0.19	67 ± 4	0.41 ± 0.26	76 ± 3	0.05 ± 0.03
	0.25	62 ± 3	0.34 ± 0.29	71 ± 3	0.37 ± 0.14
	0.32	66 ± 3	0.15 ± 0.14	73 ± 3	0.17 ± 0.13
	0.38	58 ± 5	0.11 ± 0.04	68 ± 3	0.04 ± 0.03
Herringbone	0.051	52 ± 8	0.20 ± 0.04	-	-
(glass)	0.10	53 ± 5	0.23 ± 0.06	140 ± 62	0.21 ± 0.17
	0.20	52 ± 3	0.17 ± 0.02	112 ± 17	0.20 ± 0.05
	0.31	53 ± 2	0.19 ± 0.02	109 ± 11	0.23 ± 0.15
	0.41	52 ± 4	0.20 ± 0.02	103 ± 6	0.31 ± 0.20
	0.51	50 ± 5	0.22 ± 0.01	113 ± 8	0.21 ± 0.02
	0.61	46 ± 13	0.27 ± 0.04	112 ± 8	0.15 ± 0.06
Herringbone	0.014	171 ± 23	0.09 ± 0.02	192 ± 20	0.17 ± 0.09
(plastic)	0.028	147 ± 21	0.11 ± 0.05	183 ± 30	0.33 ± 0.03
	0.042	142 ±34	0.10 ± 0.02	179 ± 12	0.20 ± 0.13
	0.069	133 ± 39	0.10 ± 0.02	181 ± 3	0.13 ± 0.09
	0.083	125 ± 26	0.12 ± 0.05	175 ± 8	0.23 ± 0.11
	0.14	133 ± 35	0.12 ± 0.02	160 ± 17	0.12 ± 0.10
	0.28	118 ± 18	0.13 ± 0.03	132 ± 7	0.12 ± 0.04
	0.42	73 ± 10	0.16 ± 0.03	115 ± 13	0.14 ± 0.09
	0.56	63 ± 11	0.22 ± 0.10	108 ± 7	0.12 ± 0.04
	0.69	55 ± 10	0.26 ± 0.11	108 ± 3	0.13 ± 0.04
Impact jet KM-3	0.12	167 ± 30	0.16 ± 0.03	155 ± 19	0.06 ± 0.03
	0.24	141 ± 13	0.17 ± 0.01	138 ± 5	0.08 ± 0.01
	0.48	77 ± 8	0.23 ± 0.05	111 ± 7	0.09 ± 0.02
	0.71	44 ± 10	0.26 ± 0.06	98 ± 12	0.09 ± 0.03
	0.94	27 ± 12	0.37 ± 0.12	80 ± 7	0.13 ± 0.08
	1.18	24 ± 6	0.28 ± 0.06	66 ± 11	0.21 ± 0.10
	2.36	18 ± 6	0.43 ± 0.16	50 ± 3	0.25 ± 0.16
	3.54	19 ± 7	0.46 ± 0.16	63 ± 14	0.19 ± 0.08
	4.72	26 ± 13	0.52 ± 0.42	64 ± 10	0.17 ± 0.09
Impact jet KM-5	0.09	185 ± 24	0.17 ± 0.04	169 ± 18	0.09 ± 0.04
	0.17	163 ± 41	0.16 ± 0.04	148 ± 20	0.09 ± 0.03

	0.35	126 ± 33	0.22 ± 0.03	131 ± 16	0.07 ± 0.03
	0.52	94 ± 12	0.25 ± 0.03	117 ± 18	0.09 ± 0.03
	0.70	70 ± 18	0.25 ± 0.04	96 ± 11	0.11 ± 0.03
	0.87	55 ± 19	0.29 ± 0.04	85 ± 22	0.14 ± 0.03
	1.73	32 ± 9	0.36 ± 0.15	58 ± 7	0.24 ± 0.07
	2.60	22 ± 3	0.35 ± 0.19	61 ± 11	0.22 ± 0.04
	3.46	20 ± 6	0.35 ± 0.19	88 ± 25	0.17 ± 0.04

Table S2. ζ-potential values for selected NP preparations.

Mixer	Flow speed	PLGA	PMMA
	($m.s^{-1}$)	ζ-potential (mV)	ζ-potential (mV)
Manual	-	-36 ± 2	-19 ± 2
Impact jet KM-3	0.24	-32 ± 6	-26 ± 7
	2.36	-34 ± 8	-23 ± 3

Table S3. Stability of selected NP preparations over time values.

Mixer	Flow speed	PLGA, size (nm)			PMMA, size (nm)		
	($m.s^{-1}$)	0 h	1 h	24 h	0 h	1 h	24 h
Manual	-	57 ± 3	54 ± 4	56 ± 5	89 ± 2	90 ± 2	93 ± 4
Impact jet KM-3	0.24	132 ± 7	127 ± 7	127 ± 10	169 ± 10	173 ± 11	172 ± 12
	2.36	18 ± 3	19 ± 5	20 ± 5	66 ± 3	84 ± 4	80 ± 4

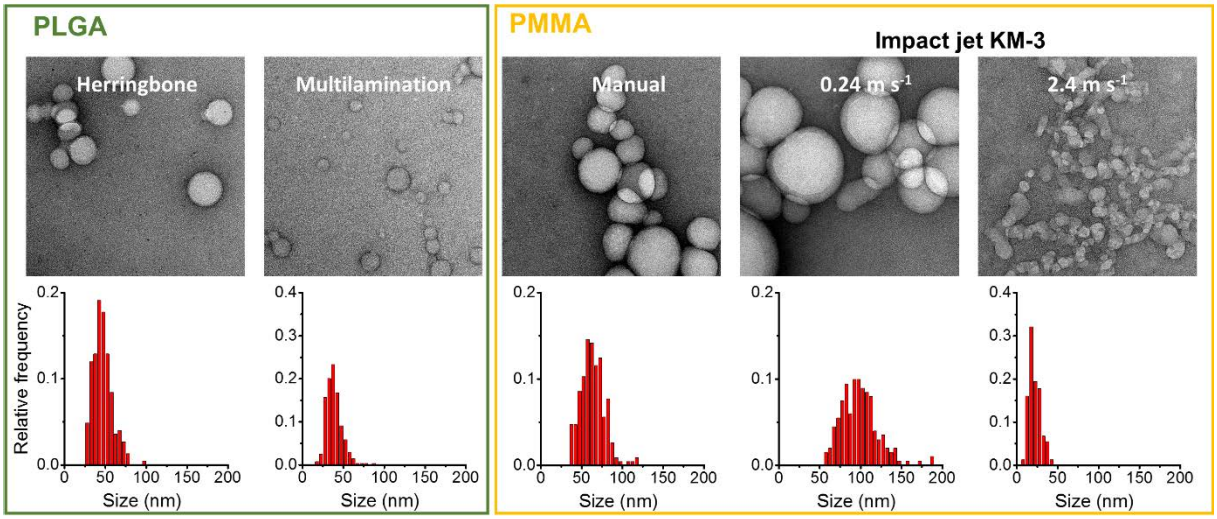

Figure S1. Analysis of NPs using TEM. Representative TEM images for different conditions of particle preparation are given above (scale bar corresponds to 100 nm), and the particle size distributions as obtained from >200 particles per condition are given below.

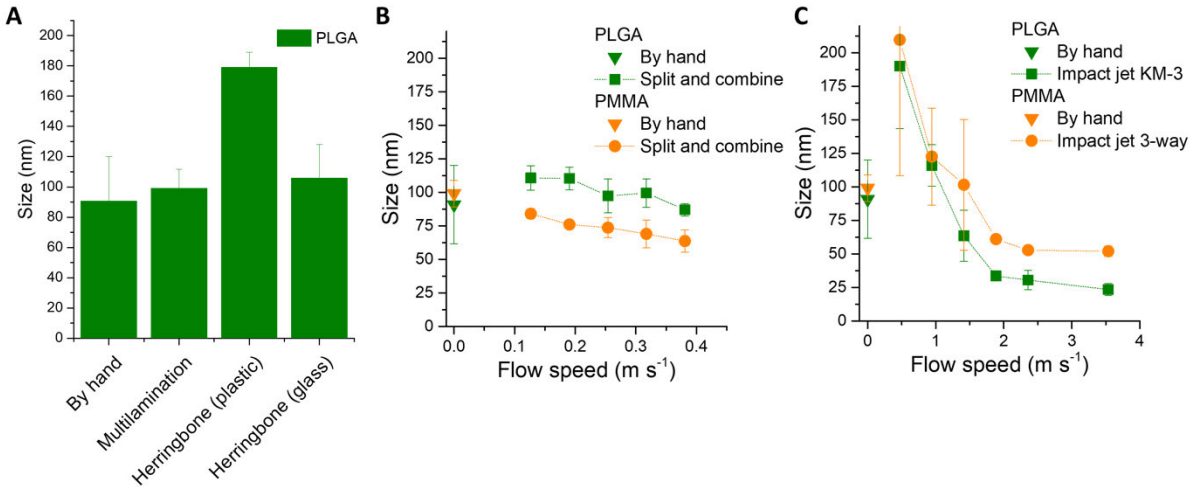

Figure S2. Sizes of dye-loaded NPs obtained using different mixers and flow speeds as measured by DLS. The values correspond to the mean of the volume average from at least three measurements. Error bars give the standard deviation.

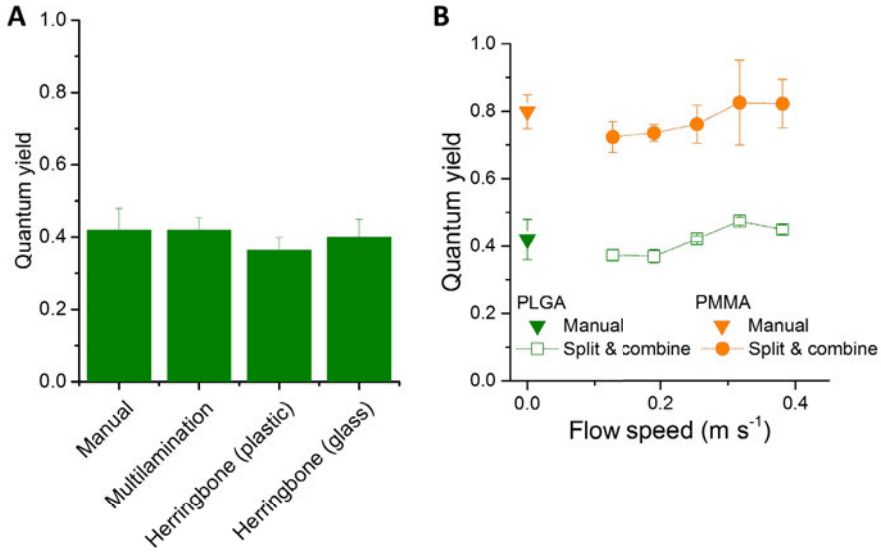

Figure S3. Quantum yields for NPs with 5wt% of R18/F5-TPB: (A) PLGA NPs prepared manually and with different mixers under optimum conditions. (B) PLGA and PMMA NPs prepared with the split & (re)combine mixer at different flow speeds. Average values over at least three independent preparations are given and the error bars correspond to the standard deviation.

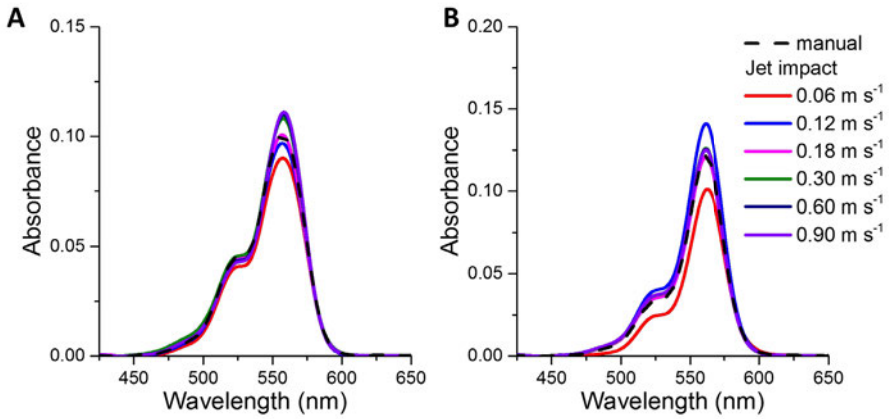

Figure S4. Absorbance spectra of dye-loaded PLGA (A) and PMMA (B) NPs prepared manually or by the KM-3 mixer.

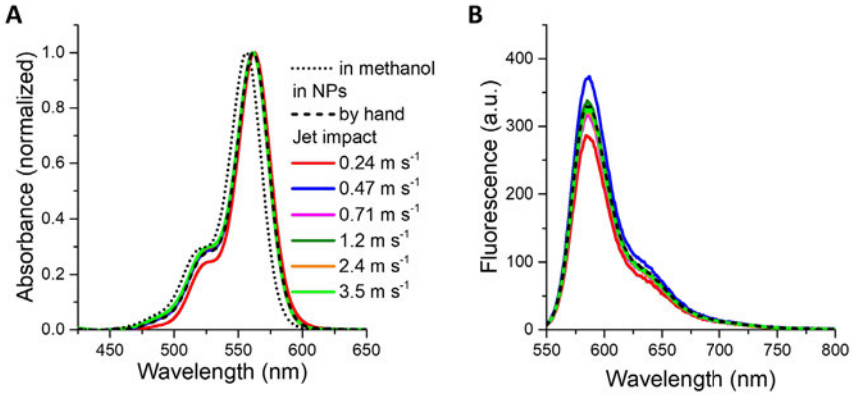

Figure S5. Absorbance (A) and emission spectra (B) of PMMA NPs with 5wt% of R18/F5-TPB prepared by hand or using the impact jet mixer at different flow speeds. Absorbance spectra in (A) are normalized to visualize changes in their shape; the spectra of the dye salt in methanol is given for comparison. The emission spectra in (B) are all recorded using the same settings and for the same global fluorophore concentration.